Earliest land plants created modern levels of atmospheric oxygen

Timothy M. Lenton[a,1], Tais W. Dahl[b], Stuart J. Daines[a], Benjamin J. W. Mills[a,c], Kazumi Ozaki[d], Matthew R. Saltzman[e], and Philipp Porada[f]

[a]Earth System Science, College of Life and Environmental Sciences, University of Exeter, Exeter EX4 4QE, United Kingdom; [b]Natural History Museum of Denmark, University of Copenhagen, DK-1350 Copenhagen, Denmark; [c]School of Earth and Environment, University of Leeds, Leeds LS2 9JT, United Kingdom; [d]School of Earth and Atmospheric Sciences, Georgia Institute of Technology, Atlanta, GA 30332-0340; [e]School of Earth Sciences, Ohio State University, Columbus, OH 43214; and [f]Department of Environmental Science and Analytical Chemistry, Stockholm University, SE-114 18 Stockholm, Sweden

Edited by Mark H. Thiemens, University of California at San Diego, La Jolla, CA, and approved July 11, 2016 (received for review March 23, 2016)

The progressive oxygenation of the Earth's atmosphere was pivotal to the evolution of life, but the puzzle of when and how atmospheric oxygen (O_2) first approached modern levels (∼21%) remains unresolved. Redox proxy data indicate the deep oceans were oxygenated during 435–392 Ma, and the appearance of fossil charcoal indicates O_2 >15–17% by 420–400 Ma. However, existing models have failed to predict oxygenation at this time. Here we show that the earliest plants, which colonized the land surface from ∼470 Ma onward, were responsible for this mid-Paleozoic oxygenation event, through greatly increasing global organic carbon burial—the net long-term source of O_2. We use a trait-based ecophysiological model to predict that cryptogamic vegetation cover could have achieved ∼30% of today's global terrestrial net primary productivity by ∼445 Ma. Data from modern bryophytes suggests this plentiful early plant material had a much higher molar C:P ratio (∼2,000) than marine biomass (∼100), such that a given weathering flux of phosphorus could support more organic carbon burial. Furthermore, recent experiments suggest that early plants selectively increased the flux of phosphorus (relative to alkalinity) weathered from rocks. Combining these effects in a model of long-term biogeochemical cycling, we reproduce a sustained +2‰ increase in the carbonate carbon isotope ($\delta^{13}C$) record by ∼445 Ma, and predict a corresponding rise in O_2 to present levels by 420–400 Ma, consistent with geochemical data. This oxygen rise represents a permanent shift in regulatory regime to one where fire-mediated negative feedbacks stabilize high O_2 levels.

oxygen | Paleozoic | phosphorus | plants | weathering

After the well-defined "Great Oxidation Event" 2.45–2.32 Ga, the trajectory of atmospheric oxygen is deeply uncertain (1, 2). Many recent studies, reviewed in refs. 3–5 have argued for a Neoproterozoic oxygenation event (>550 Ma)—of uncertain cause—and have linked it to the rise of animals, but this has been questioned given a lack of change in iron speciation ocean redox proxy data (6). Some models predict pO_2 ∼1 present atmospheric level (PAL) already in the Early Paleozoic (7, 8), but this is at odds with data for widespread ocean anoxia (6, 9). The COPSE model we adapt here (10) predicts Early Paleozoic pO_2 ∼0.2–0.5 PAL consistent with redox proxy data but, like the other models (7, 8), it does not predict a rise in oxygen until the advent of forests starting ∼385 Ma, and continuing until ∼300 Ma, which is too late to explain marked changes in geochemical data that occur before ∼390 Ma (Fig. 1). The first appearance of fossil charcoal in the Late Silurian (11) and its ongoing occurrence through the Devonian (12) (Table S1), albeit rare and at low concentrations, indicates O_2 > 15–17% (vol) of the atmosphere (13) (or O_2 > ∼0.7 PAL assuming a constant N_2 reservoir) already by ∼420–400 Ma. [Under ideal conditions of ultradry fuel and forced airflow, smoldering fires may be sustained at O_2 > 10%, but this is not believed to be possible under natural conditions (14).] The molybdenum isotope record (9) indicates a fundamental shift in the redox state of the deep ocean from widespread anoxia to widespread oxygenation sometime during 435–392 Ma (between the Early Silurian and the Middle Devonian). This ocean oxygenation is also supported by a Silurian increase in the C/S ratio of shales (15), and a shift in iron speciation data sometime during 435–387 Ma (6).

The persistent oxygenation of the ocean and appearance of charcoal can be explained by a rise in atmospheric oxygen occurring by ∼400 Ma; this could be due to a persistent increase in oxygen source—considered here—or a decrease in oxygen sink (16), leading to a reorganization of the Earth's surface redox balance at a higher steady-state level for atmospheric O_2. The major long-term source of oxygen to the atmosphere is the burial of organic carbon in sedimentary rocks (which represents the net flux of photosynthesis minus various pathways of respiration and oxidation). Increases in global organic carbon burial are recorded as positive shifts in the isotopic composition of carbonate rocks ($\delta^{13}C$). Consistent with a rise in oxygen, the carbon isotope record (17) (Fig. 1) indicates a fundamental shift in baseline from ≤0‰ before the Late Ordovician to ∼2‰ from ∼445 Ma onward. Though there are many subsequent $\delta^{13}C$ fluctuations, including drops back to 0‰, for example, at ∼400 Ma, the long-term mean $\delta^{13}C$ remains ∼2‰ throughout the rest of the Paleozoic, the Mesozoic, and the Early Cenozoic (17), indicating a sustained increase in global organic carbon burial. Such a permanent shift requires a unidirectional driver that kicked in during the mid-Paleozoic. The evolution of land plants is the obvious candidate, with the first nonvascular plants (ancestors of extant mosses, liverworts, and hornworts) colonizing the land in the Middle to Late Ordovician (∼470–445 Ma), followed by the first vascular plants in the Silurian (∼445–420 Ma) and Early Devonian (∼420–390 Ma; Fig. 1) (18, 19).

Significance

The rise of atmospheric oxygen over Earth's history has received much recent interdisciplinary attention. However, the puzzle of when and how atmospheric oxygen reached modern levels remains unresolved. Many recent studies have argued for a major oxygenation event—of uncertain cause—in the Neoproterozoic Era >541 Ma, enabling the rise of animals. Previous modelling work has predicted a late Paleozoic oxygen rise (<380 Ma) due to the rise of forests. Here we show that neither scenario is correct. Instead, the earliest plants, which colonized the land from 470 Ma onward, first increased atmospheric oxygen to present levels by 400 Ma, and this instigated fire-mediated feedbacks that have stabilized high oxygen levels ever since, shaping subsequent evolution.

Author contributions: T.M.L. designed research; T.M.L. and P.P. performed research; T.M.L., S.J.D., B.J.W.M., K.O., and P.P. contributed new reagents/analytic tools; T.M.L., T.W.D., K.O., M.R.S., and P.P. analyzed data; and T.M.L. wrote the paper.

The authors declare no conflict of interest.

This article is a PNAS Direct Submission.

[1]To whom correspondence should be addressed. Email: t.m.lenton@exeter.ac.uk.

This article contains supporting information online at www.pnas.org/lookup/suppl/doi:10.1073/pnas.1604787113/-/DCSupplemental.

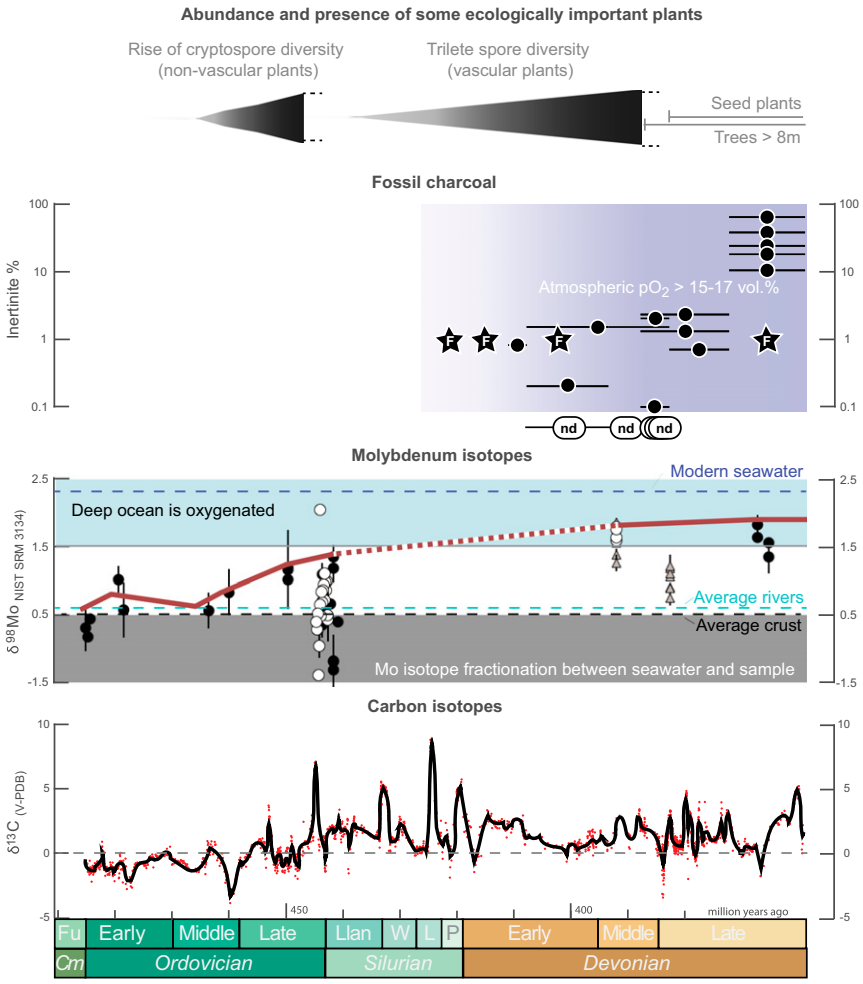

Fig. 1. Global changes during the Ordovician, Silurian, and Devonian periods. The rise of nonvascular plants [indicated by cryptospore diversity (32)] and then vascular plants [indicated by trilete spore diversity (18)] overlaps with the first appearances of fossil charcoal (Table S1). F, fossils; black dots, inertinite in coal; nd, none detected. Molybdenum isotope data (9) indicate oxygenation of the deep ocean, following an uncertain trajectory ∼440–390 Ma. Black circles indicate euxinic shales as defined by Fe speciation; white circles, euxinic shales as defined by Mo enrichment; gray triangles, ferruginous shales as defined by Fe speciation; blue area, isotope offset from oceanic input that requires a substantial Mn oxide sink in the deep oceans. The carbonate carbon isotope record (17) (red dots, black line is a smoothed spline fit) indicates elevated organic carbon burial ($\delta^{13}C$ ∼2‰) from ∼445 Ma. Cm, Cambrian; Fu, Furongian; Llan, Llandovery; L, Ludlow; P, Pridoli; W, Wenlock.

Here we hypothesize that the evolution of these earliest land plants permanently increased organic carbon burial, causing atmospheric oxygen to approach modern levels by ∼400 Ma and creating a new dynamically stable steady state for the oxygen cycle (where the major long-term O_2 sink from oxidative weathering of ancient organic carbon increased to counterbalance the increased O_2 source). In simple terms, on long timescales, the global organic carbon burial flux is determined by the supply flux of the ultimate limiting nutrient phosphorus from weathering and the (molar) ratio of carbon-to-phosphorus in material that is buried

$$\text{P weathering flux} \times C_{\text{organic}}/P_{\text{total}}\ \text{burial ratio} = C_{\text{organic}}\ \text{burial flux}.$$

Land plants typically have a much higher molar C/P ratio (∼1,000) than marine organic matter (∼100) due to carbon-rich but phosphorus-poor structural compounds such as sporopollenin, lignin, and, in their fungal mycorrhizal symbionts, chitin; therefore, they can support an increased organic carbon burial flux for the same P weathering flux. The P weathering flux is partly tied to bulk silicate weathering, for example, due to the dissolution of apatite inclusions in silicate rocks, and the silicate weathering flux of alkalinity is in turn set by negative feedback in the long-term carbon cycle, so is ultimately controlled by the degassing input of CO_2 on timescales ≥1 My (7, 10). However, plants and their associated mycorrhizal fungi can increase phosphorus weathering (20–22), and this could be sustained on longer timescales if they preferentially weather phosphorus relative to alkalinity.

In existing models, the evolution of trees starting ∼385 Ma is assumed to have led to the burial of high C/P organic material in coal swamps (7, 8, 10), potentially augmented by increased phosphorus weathering rates (10). The Carboniferous–Permian peak in coal production has often been attributed to the evolution of lignin synthesis and a lag before the evolution of fungal degradation of lignin (23), but recent work has questioned this (24). Earlier plants possessed lignified "woody" tissue (25), with precursor structures existing in marine algae before the transition to land (26), and lignin-degrading fungi potentially present before the Carboniferous (24). Carboniferous coals are not dominated by lignin; instead, their accumulation was controlled by a combination of climate and tectonics supporting the creation and sedimentary preservation of peat bogs (24, 27). Given that earlier plants developed peatlands (28), and had rock-weathering capabilities (20, 21), they could also have affected the global carbon cycle (18, 20).

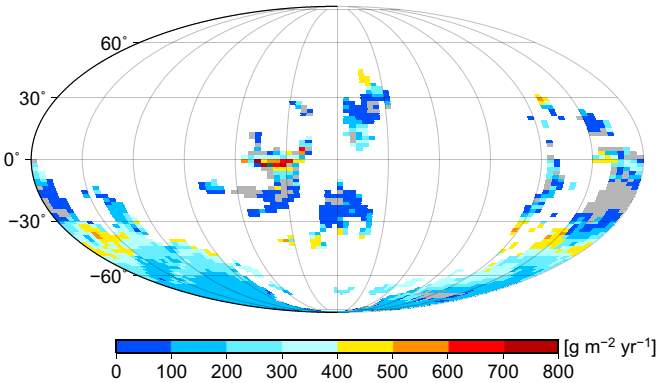

Fig. 2. Predicted Late Ordovician (445 Ma) NPP. Result from ecophysiological model of cryptogamic vegetation cover driven by simulated Late Ordovician (445 Ma) climate, atmospheric CO_2 = 8 PAL, and atmospheric O_2 = 0.6 PAL (14 vol%), with no ice sheet mask. Simulated global NPP = 18.7 GtC·y^{-1}.

Results and Discussion

To test our hypothesis, we revised the COPSE biogeochemical model (10) to better capture the early rise of plants and examine under what conditions it could explain the geochemical data (persistent rise to $\delta^{13}C$ ~2‰ and the appearance of charcoal). The original baseline model (10) predicts early Paleozoic O_2 ~0.23 PAL at a reference time of 445 Ma, supported by an organic carbon burial flux of ~4×10^{12} mol·y^{-1} (about half the present-day value) with $\delta^{13}C$ = 0.03‰. In this stable state, oxidative weathering of ancient organic carbon is correspondingly reduced and its sensitivity to changes in O_2 provides a key negative feedback stabilizing O_2. Key assumptions going into altering the forcing of the model are the global extent and associated productivity of early plants, the C/P ratio of plant material that was buried, and their effect (if any) on phosphorus weathering. To help parameterize these factors we drew on a mixture of experiments, existing data, and more detailed spatial modeling.

We used a trait-based spatial model of cryptogamic vegetation (i.e., bryophyte and lichen) cover (29, 30) driven by Late Ordovician climate simulations (31) at different atmospheric CO_2 levels to predict the potential global net primary productivity (NPP) of the early plant biosphere (32). At atmospheric CO_2 = 8 PAL, consistent with Late Ordovician glaciations (20), predicted global NPP is ~19 GtC·y^{-1} (GtC, billion metric tons of carbon) (Fig. 2), ~30% of today. Predicted NPP is sensitive to variations in CO_2 and climate (Fig. S1), ice sheet cover (Fig. S2), and O_2 (Table S2), but is consistently higher than the 4.3 GtC·y^{-1} (7% of today) estimated elsewhere (33). In the original COPSE model (10), predicted NPP only reaches ~5% of today's value in the Late Ordovician and Silurian, but when we assume a stronger Late Ordovician phase of land colonization by nonvascular plants (following ref. 20; *SI Materials and Methods*), then COPSE predicts global NPP 30–40% of today (Fig. 3*A*), consistent with the detailed spatial model. In COPSE, this advent of early land plants alone, with no assumed effect on weathering fluxes, and assumed C/P = 1,000, increases total organic carbon burial by ~25%, $\delta^{13}C$ by 0.5‰, and atmospheric O_2 by 0.11 PAL (Fig. 3, blue).

We undertook a literature review of molar C/P ratios in extant bryophytes (Table S3) to test whether C/P = 1,000 is a reasonable

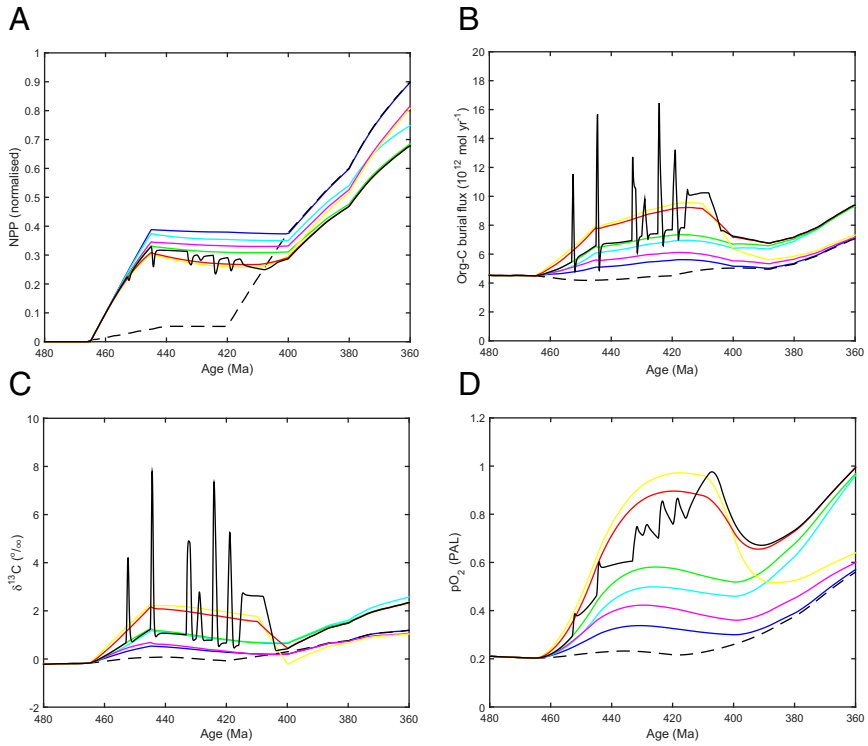

Fig. 3. Predictions of mid-Paleozoic global carbon cycle change due to early plants from the updated COPSE model. (*A*) NPP. (*B*) Organic carbon burial (both terrestrial and marine-derived material). (*C*) Carbonate carbon isotope record ($\delta^{13}C$). (*D*) Atmospheric O_2. Note that fossil charcoal 420–400 Ma indicates O_2 > 0.66–0.77 PAL. (Further results of the same model runs are in Figs. S3 and S5.) Black dashed line indicates original baseline model run; blue, early plant colonization (C/P = 1,000); cyan, early plant colonization + C/P = 2,000; magenta, early plant colonization + biotic effects on silicate weathering (C/P = 1,000); green, early plant colonization + C/P = 2,000 + biotic effects on silicate weathering; yellow, early plant colonization + biotic effects on silicate weathering + 50% increase in P weathering; red, early plant colonization + C/P = 2,000 + biotic effects on silicate weathering + 25% increase in P weathering; black, early plant colonization + C/P = 2,000 + biotic effects on silicate weathering + spikes of P weathering.

assumption for early plants, and this gives a range of C/P = 800–4,300 with a mean of C/P ∼1,900. Furthermore, Early Devonian coaly shales indicate extensive peatlands 410–400 Ma and have C/N of 44–119 (28), comparable to that in modern peatlands where N/P and C/P ratios tend to increase with depth to C/P > 3,000 (34). Taken together, these data suggest that assuming C/P = 1,000 for early plants is conservative. If instead we assume that buried early plant matter had C/P = 2,000, then given their productivity, even with no effect on weathering fluxes, this increases global organic carbon burial by ∼50%, $\delta^{13}C$ by 1.1‰, and atmospheric O_2 by 0.27 PAL (Fig. 3, cyan).

Early plants could also have had a significant effect on weathering fluxes (20), because they and their fungal mycorrhizal symbionts evolved means of accessing rock-bound nutrients, notably phosphorus. Experimental work (20) has shown that a modern nonvascular plant, the moss *Physcomitrella patens*, amplifies the weathering of Ca ions 1.4- to 3.6-fold and Mg ions 1.5- to 5.4-fold from silicate rocks (granite–andesite), and amplifies the weathering of phosphorus from granite ∼24-fold (range 15–43; *Materials and Methods*). Subsequent experiments (21) with the modern liverwort *Marchantia paleacea* found a 2.5- to 7-fold amplification of Ca weathering and a 9- to 13-fold amplification of P weathering from basalt. Both studies thus indicate preferential weathering of P relative to Ca and Mg (and corresponding alkalinity). The presence of these rock-weathering capabilities in two early diverging lineages (mosses and liverworts) suggests it is an ancestral trait. It has been argued (21, 33) that such large measured local effects would not have scaled up to significant global effects, because of low global NPP (33) and a limited depth of influence in the soil (21). However, we estimate much higher global NPP (Fig. 2) and weathering potential (32). We also note that extensive shallow water phosphate deposits in the Late Ordovician (35) indicate a marked increase in phosphorus input to the ocean (20).

If we include in COPSE an effect of early plants on silicate weathering following ref. 20, assuming C/P = 1,000, this increases organic carbon burial by ∼35%, $\delta^{13}C$ by 0.7‰, and O_2 by 0.18 PAL (Fig. 3, magenta). The effect on O_2 is constrained because atmospheric CO_2 and temperature are reduced (20) such that the silicate weathering flux (and associated phosphorus flux) continues to match the degassing flux of CO_2 (Fig. S3). However, increases in carbonate weathering (enhanced by plants) and oxidative weathering (due to the rise in O_2) increase the overall phosphorus weathering flux, roughly doubling the O_2 rise due to terrestrial production of high C/P material alone. Assuming that buried early plant matter had a higher C/P = 2,000 causes larger increases in total organic carbon burial ∼60%, $\delta^{13}C$ + 1.2‰, and atmospheric O_2 + 0.35 PAL (Fig. 3, green).

However, to reproduce the observed $\delta^{13}C$ +2‰ shift requires the inclusion of some selective weathering of phosphorus by early plants. Assuming that early plants caused a sustained 50% increase in phosphorus weathering relative to bulk rock dissolution, with C/P = 1,000, increases total organic carbon burial by ∼95%, $\delta^{13}C$ by 2.2‰, and O_2 by 0.74 PAL (to 0.97 PAL at 417 Ma; Fig. 3, yellow). Assuming a sustained 25% increase in phosphorus weathering relative to bulk rock and C/P = 2,000 increases organic carbon burial by ∼90%, $\delta^{13}C$ by 2.1‰, and O_2 by 0.67 PAL (Fig. 3, red). Alternatively, a series of P weathering spikes designed to reproduce the observed sequence of positive $\delta^{13}C$ excursions (Fig. 1), combined with C/P = 2,000, produces a series of spikes in organic carbon burial and a peak increase of O_2 of 0.72 PAL at 407 Ma (Fig. 3, black). We hypothesize that these assumed weathering spikes could reflect phases of plant colonization (20, 36) followed by the establishment of phosphorus recycling ecosystems (20). However, direct evidence linking a phase of land colonization to enhanced weathering and a positive $\delta^{13}C$ excursion has only thus far been established for the Silurian–Devonian boundary excursion (36). Therefore, alternative hypotheses for short-lived positive $\delta^{13}C$ excursions should also be considered.

Regarding the simulated long-term ∼2‰ rise in $\delta^{13}C$, this is smaller than would be expected from standard application of the simplified formula: $\delta^{13}C(\text{ocean}) = \delta^{13}C(\text{river}) + f_{org}\bullet\varepsilon$, where f_{org} is the fraction of carbon buried as organic matter, ε is the fractionation between carbonates and organic matter, and both ε and $\delta^{13}C$(river) are usually assumed to be constant. In our COPSE simulations there is a fully interactive isotope mass balance, and these terms are not constant. The approximate doubling of organic carbon burial (with roughly constant carbonate burial) represents an increase from f_{org} = 0.18 to f_{org} = 0.31. However, the increase in burial of isotopically light organic carbon is counteracted by an increase in the oxidative weathering of isotopically light organic carbon, which lowers the $\delta^{13}C$ of riverine input to the ocean from approximately −5‰ to approximately −7.5‰, which is in turn partially counteracted by an increase in fractionation between carbonates and organic matter from ε ∼27 to ∼30‰, due to increasing O_2 (somewhat counteracted by declining CO_2).

Sensitivity analyses (*SI Materials and Methods*) indicate that our results are robust. Varying the uplift and degassing forcing of the model within plausible bounds only causes ±0.08 PAL variation in O_2 about the initial state (Fig. S4), although it does cause the effect of the same early plant forcing scenario to range over +0.4 to 1.0 PAL O_2 (Table S4). Including an additional negative feedback on O_2, from increased marine organic C/P burial ratios under anoxic waters (37), increases its initial early Paleozoic level to 0.54 PAL and reduces the effect of the same biological forcing scenarios on O_2 by ∼10–30%, giving a maximum increase of +0.63 PAL (Table S5). However, because the initial O_2 is now higher, the final O_2 is also higher in all cases, and even scenarios without selective weathering of phosphorus could explain the appearance of charcoal (O_2 > ∼0.7 PAL).

Our model makes additional predictions that can be tested against geochemical data—notably, it predicts a decline in pyrite sulfur burial and associated drop in $\delta^{34}S$ and increases in seawater SO_4 concentration and C/S burial ratio with the rise of the earliest plants (Fig. S5). This finding is broadly consistent with the sulfur isotope ($\delta^{34}S$) record (38–40), which shows a marked decline through the Silurian–Early Devonian from ∼30 to ∼18‰, although available data also suggest an earlier Late Ordovician–Early Silurian rise from ∼25 to ∼30‰, which the present model does not capture. The model is consistent with proxy reconstructions of seawater SO_4 concentration, which suggest an Ordovician–Silurian rise from ∼6 to ∼10 mM (41), and with a Silurian increase in the molar C/S ratio of shales from ∼5 to ∼16 (15).

Other processes not yet included in the model warrant future consideration—for example, the effect of increasing atmospheric mass on climate (42) and the effect of weathering forcing scenarios on $\delta^{7}Li$ and $^{87}Sr/^{86}Sr$, which enable additional tests against data.

Conclusion

Our model can only reproduce Paleozoic geochemical data if the rise of the earliest land plants caused a major oxygenation event of the Earth's atmosphere and oceans by ∼400 Ma. We attribute this mid-Paleozoic oxygenation event to a persistent global increase in organic carbon burial supported by the high C/P ratio of early land plant material, augmented by a plant-driven increase in P weathering flux relative to the weathering flux of alkalinity. The $\delta^{13}C$ record suggests this increase in organic carbon burial was essentially permanent, producing a new dynamically stable state for atmospheric O_2. In this new steady state, oxidative weathering was increased (becoming less sensitive to variations in O_2) and new fire-mediated negative feedbacks on O_2 were instigated that have played a key role in stabilizing atmospheric O_2 concentration up to the present day (22, 43). For the earliest land plants to be responsible for such a major mid-Paleozoic oxygenation event requires that they were much more productive and globally

extensive than has been previously assumed (7, 10, 33). This hypothesis makes testable predictions with regard to effects on other biogeochemical cycles, notably sulfur; if it stands up to further scrutiny, we can then infer that the earliest land plants created a stable oxygen-rich atmosphere that was necessary for the subsequent evolution of large, mobile, intelligent animals with a high respiratory oxygen demand, including ourselves.

Materials and Methods

Data Compilation. The early charcoal record (Table S1) was compiled from the literature (11, 12, 28, 44–72) using existing compilations (12, 44–47) and checking them where possible against the original sources. This process involved some reconciling of disparate results between existing compilations and revision of some erroneous quoted values. Where recalculations were warranted, inertinite percentages were calculated on a mineral matter-free (mmf) basis, following refs. 45 and 47.

The molybdenum isotope record from marine shales was updated from ref. 9 with data from refs. 73 and 74. Uncertainties shown in Fig. 1 represent 2 SD of the mean (analytical precision) plus the propagated uncertainty from matching in-house reference materials to the universal standard NIST SRM 3136 where seawater display $\delta^{98/95}$Mo = 2.3‰ (75, 76). The redox state of the host shales was determined using either Fe speciation or Mo enrichment proxies. Euxinic shales are defined (77) by the Fe speciation proxy when FeHR/FeT > 0.38 and FeP/FeHR > 0.7 (black circles in Fig. 1). Euxinic shales are defined (78, 79) by the Mo enrichment proxy when Mo > 25 ppm (white circles in Fig. 1). Ferruginous shales (77) are defined by the Fe speciation proxy when FeHR/FeT > 0.38 and FeP/FeHR < 0.7.

The carbon isotope record (17) was fitted with a smoothed spline function in MATLAB; spline = csaps(age, δ^{13}C, ρ), where $\rho = 0.99$ (close to data, but the curve in Fig. 1 does not go through each data point).

The C/P ratio of extant bryophytes (Table S3) was compiled from data in the literature (34, 80–88). Where only values of mg P/g biomass were available, a value of mg C/g biomass = 430 was assumed based on the mean value across six bryophyte species from ref. 89. Results for molar C/P ratios are given to two significant figures, given the uncertainty in the input data, except where authors themselves provide more precise values.

Ecophysiological Model of Cryptogamic Vegetation. We used a trait-based spatial model of cryptogamic vegetation (i.e., bryophyte and lichen) cover to estimate the potential global NPP of the early nonvascular plant biosphere (29, 30). The Late Ordovician (445 Ma, Hirnantian stage) setup of the model is fully described elsewhere (32). The model is driven by existing Late Ordovician climate simulations (31), conducted at a range of different atmospheric CO_2 and O_2 concentrations. Initially, we assume atmospheric O_2 = 0.6 PAL (~14 vol.%) at 445 Ma, which is consistent with COPSE model simulations (Fig. 3*D*) that go on to produce O_2 levels consistent with the fossil charcoal record. We also initially assume atmospheric CO_2 = 8 PAL, which is a widely quoted value consistent with the occurrence of Hirnantian glaciations at 445 Ma (20), and consistent with COPSE model simulations that assume an effect of early plants on silicate weathering following ref. 20. We explored the sensitivity of predicted global NPP to variations in atmospheric CO_2 and corresponding climate state (Fig. S1), to constraining vegetation cover with extensive Late Ordovician ice sheet cover (Fig. S2), and to varying O_2 in combination with CO_2 (Table S2). The relatively high global NPP results obtained are consistent with present-day cryptogamic covers providing ~7% of global NPP, despite making up only 1% of terrestrial vegetation by mass (90) and being restricted to relatively resource-poor habitats, while also operating in an atmosphere with a low CO_2/O_2 ratio.

Experimental P Weathering Calculation. In our previously reported (20) weathering experiments with granite, the mean amounts of phosphate weathered into aqueous solution were as follows: control microcosms = 0.0137 μmol P, biotic microcosms = 0.0726 μmol P. The mean moss biomass in the biotic microcosms was 14.390 mg, which assuming 0.43 gC/g biomass and C/P = 2,000 (Table S3) suggests 0.26 μmol P in biomass, or for C/P = 1,000–4,000, 0.13–0.52 μmol P in biomass; this gives a biotic P weathering amplification factor ~24 (range 15–43), whereas previously we suggested up to 60 (20). Clearly these estimates are dominated by the unmeasured P content of biomass. However, the P weathering amplification factor has to be >5.3 (the ratio of dissolved phosphate entering solution in microcosms with moss to those without), which is already considerably greater than the amplification factors for Ca = 1.4 and Mg = 1.5 from granite, indicating selective weathering of P.

COPSE Model. We used the COPSE model (10, 20) to study the effects of the early rise of land plants on the coupled biogeochemical cycles of C, O, N, P, and S, including the δ^{13}C record. The model is described in full in ref. 10, and the version used here incorporates the changes in model structure described in ref. 20. The model has several forcing parameters, including solar luminosity; the geological factors degassing (*D*) and uplift (*U*); and the biological forcing factors evolution/colonization (*E*), enhancement of weathering (*W*), selective phosphorus weathering (*F*), and changes to the C/P burial ratio of terrestrially derived material (*CP*). The geologic and biologic forcing factors are all normalized to 1 at the present day, except C/P = 1,000 at present day. Our overall modeling strategy was to try and reproduce key changes in the δ^{13}C record with plausible biological and geological forcing scenarios, constrained where possible by available data. We focused initially on altering the biological forcing scenario while using the original geological forcing scenario. Then, in a sensitivity analysis, we considered uncertainty in geologic forcing (91), and alternative initial conditions (altering the feedback structure of the model). The forcing scenarios and sensitivity analyses are detailed in the *SI Materials and Methods*.

ACKNOWLEDGMENTS. We thank two anonymous referees for insightful comments that improved the manuscript. Support for this work was provided by Leverhulme Trust Grant RPG-2013-106 (to T.M.L., S.J.D., and B.J.W.M.); NERC Grant NE/I005978/2 (to T.M.L.); a Royal Society Wolfson Research Merit Award (to T.M.L.); a University of Leeds Academic Fellowship (to B.J.W.M.); and VILLUM Foundation Grant VKR023127 (to T.W.D.).

1. Canfield DE (2014) Proterozoic Atmospheric Oxygen. *Treatise on Geochemistry*, eds Holland HD, Turekian KK (Elsevier Science, Oxford), 2nd Ed, Vol 6, pp 197–216.
2. Lyons TW, Reinhard CT, Planavsky NJ (2014) The rise of oxygen in Earth's early ocean and atmosphere. *Nature* 506(7488):307–315.
3. Lenton TM, Boyle RA, Poulton SW, Shields GA, Butterfield NJ (2014) Co-evolution of eukaryotes and ocean oxygenation in the Neoproterozoic era. *Nat Geosci* 7(4): 257–265.
4. Shields-Zhou GA, Och LM (2011) The case for a Neoproterozoic oxygenation event: Geochemical evidence and biological consequences. *GSA Today* 21(3):4–11.
5. Och LM, Shields-Zhou GA (2012) The Neoproterozoic Oxygenation Event: Environmental perturbations and biogeochemical cycling. *Earth Sci Rev* 110(1-4):26–57.
6. Sperling EA, et al. (2015) Statistical analysis of iron geochemical data suggests limited late Proterozoic oxygenation. *Nature* 523(7561):451–454.
7. Berner RA (2006) GEOCARBSULF: A combined model for Phanerozoic atmospheric O2 and CO2. *Geochim Cosmochim Acta* 70(23):5653–5664.
8. Berner RA, Canfield DE (1989) A new model for atmospheric oxygen over Phanerozoic time. *Am J Sci* 289(4):333–361.
9. Dahl TW, et al. (2010) Devonian rise in atmospheric oxygen correlated to the radiations of terrestrial plants and large predatory fish. *Proc Natl Acad Sci USA* 107(42): 17911–17915.
10. Bergman NM, Lenton TM, Watson AJ (2004) COPSE: A new model of biogeochemical cycling over Phanerozoic time. *Am J Sci* 304:397–437.
11. Glasspool IJ, Edwards D, Axe L (2004) Charcoal in the Silurian as evidence for the earliest wildfire. *Geology* 32(5):381–383.
12. Scott AC, Glasspool IJ (2006) The diversification of Paleozoic fire systems and fluctuations in atmospheric oxygen concentration. *Proc Natl Acad Sci USA* 103(29): 10861–10865.
13. Belcher CM, McElwain JC (2008) Limits for combustion in low O2 redefine paleoatmospheric predictions for the Mesozoic. *Science* 321(5893):1197–1200.
14. Hadden RM, Rein G, Belcher CM (2013) Study of the competing chemical reactions in the initiation and spread of smouldering combustion in peat. *Proc Combust Inst* 34(2): 2547–2553.
15. Berner RA, Raiswell R (1983) Burial of organic carbon and pyrite sulfur in sediments over phanerozoic time: A new theory. *Geochim Cosmochim Acta* 47(5):855–862.
16. Kump LR (2014) Hypothesized link between Neoproterozoic greening of the land surface and the establishment of an oxygen-rich atmosphere. *Proc Natl Acad Sci USA* 111(39):14062–14065.
17. Saltzman MR, Thomas E (2012) Carbon isotope stratigraphy. *The Geologic Time Scale*, eds Gradstein FM, Schmitz JGOD, Ogg GM (Elsevier, Boston), pp 207–232.
18. Kenrick P, Wellman CH, Schneider H, Edgecombe GD (2012) A timeline for terrestrialization: Consequences for the carbon cycle in the Palaeozoic. *Philos Trans R Soc Lond B Biol Sci* 367(1588):519–536.
19. Edwards D, Morris JL, Richardson JB, Kenrick P (2014) Cryptospores and cryptophytes reveal hidden diversity in early land floras. *New Phytol* 202(1):50–78.
20. Lenton TM, Crouch M, Johnson M, Pires N, Dolan L (2012) First plants cooled the Ordovician. *Nat Geosci* 5(2):86–89.
21. Quirk J, et al. (2015) Constraining the role of early land plants in Palaeozoic weathering and global cooling. *Proc Biol Sci*, 10.1098/rspb.2015.1115.
22. Lenton TM, Watson AJ (2000b) Redfield revisited: 2. What regulates the oxygen content of the atmosphere? *Global Biogeochem Cycles* 14(1):249–268.
23. Robinson JM (1990) Lignin, land plants, and fungi: Biological evolution affecting Phanerozoic oxygen balance. *Geology* 18(7):607–610.
24. Nelsen MP, DiMichele WA, Peters SE, Boyce CK (2016) Delayed fungal evolution did not cause the Paleozoic peak in coal production. *Proc Natl Acad Sci USA* 113(9):2442–2447.

25. Gerrienne P, et al. (2011) A simple type of wood in two Early Devonian plants. *Science* 333(6044):837.
26. Labeeuw L, Martone PT, Boucher Y, Case RJ (2015) Ancient origin of the biosynthesis of lignin precursors. *Biol Direct* 10(1):23.
27. Montañez IP (2016) A Late Paleozoic climate window of opportunity. *Proc Natl Acad Sci USA* 113(9):2334–2336.
28. Kennedy KL, et al. (2013) Lower Devonian coaly shales of northern New Brunswick, Canada: Plant accumulations in the early stages of Terrestrial colonization. *J Sediment Res* 83(12):1202–1215.
29. Porada P, Weber B, Elbert W, Poschl U, Kleidon A (2013) Estimating global carbon uptake by lichens and bryophytes with a process-based model. *Biogeosciences* 10(11): 6989–7033.
30. Porada P, Weber B, Elbert W, Pöschl U, Kleidon A (2014) Estimating impacts of lichens and bryophytes on global biogeochemical cycles. *Global Biogeochem Cycle*, 10.1002/2013GB004705.
31. Pohl A, Donnadieu Y, Le Hir G, Buoncristiani JF, Vennin E (2014) Effect of the Ordovician paleogeography on the (in)stability of the climate. *Clim Past* 10(6):2053–2066.
32. Porada P, et al. (2016) High potential for weathering and climate effects of non-vascular vegetation in the Late Ordovician. *Nat Commun*, 10.1038/ncomms12113.
33. Edwards D, Cherns L, Raven JA (2015) Could land-based early photosynthesizing ecosystems have bioengineered the planet in mid-Palaeozoic times? *Palaeontology* 58(5): 803–837.
34. Wang M, Moore TR, Talbot J, Richard PJH (2014) The cascade of C:N:P stoichiometry in an ombrotrophic peatland: from plants to peat. *Environ Res Lett* 9(2):024003.
35. Pope MC, Steffen JB (2003) Widespread, prolonged late Middle to Late Ordovician upwelling in North America: A proxy record of glaciation? *Geology* 31(1):63–66.
36. Małkowski K, Racki G (2009) A global biogeochemical perturbation across the Silurian–Devonian boundary: Ocean–continent–biosphere feedbacks. *Palaeogeogr Palaeoclimatol Palaeoecol* 276(1–4):244–254.
37. Van Cappellen P, Ingall ED (1996) Redox stabilization of the atmosphere and oceans by phosphorus-limited marine productivity. *Science* 271:493–496.
38. Prokoph A, Shields GA, Veizer J (2008) Compilation and time-series analysis of a marine carbonate δ18O, δ13C, 87Sr/86Sr and δ34S database through Earth history. *Earth Sci Rev* 87(3–4):113–133.
39. Gill BC, Lyons TW, Saltzman MR (2007) Parallel, high-resolution carbon and sulfur isotope records of the evolving Paleozoic marine sulfur reservoir. *Palaeogeogr Palaeoclimatol Palaeoecol* 256(3–4):156–173.
40. Jones DS, Fike DA (2013) Dynamic sulfur and carbon cycling through the end-Ordovician extinction revealed by paired sulfate–pyrite δ34S. *Earth Planet Sci Lett* 363: 144–155.
41. Algeo TJ, Luo GM, Song HY, Lyons TW, Canfield DE (2015) Reconstruction of secular variation in seawater sulfate concentrations. *Biogeosciences* 12(7):2131–2151.
42. Poulsen CJ, Tabor C, White JD (2015) Climate change. Long-term climate forcing by atmospheric oxygen concentrations. *Science* 348(6240):1238–1241.
43. Kump LR (1988) Terrestrial feedback in atmospheric oxygen regulation by fire and phosphorus. *Nature* 335:152–154.
44. Rimmer SM, Hawkins SJ, Scott AC, Cressler WL (2015) The rise of fire: Fossil charcoal in late Devonian marine shales as an indicator of expanding terrestrial ecosystems, fire, and atmospheric change. *Am J Sci* 315(8):713–733.
45. Glasspool IJ, Scott AC (2010) Phanerozoic concentrations of atmospheric oxygen reconstructed from sedimentary charcoal. *Nat Geosci* 3(9):627–630.
46. Diessel CFK (2010) The stratigraphic distribution of inertinite. *Int J Coal Geol* 81(4): 251–268.
47. Glasspool IJ, Scott AC, Waltham D, Pronina N, Shao L (2015) The impact of fire on the Late Paleozoic Earth system. *Front Plant Sci* 6:756.
48. Edwards D, Axe L (2004) Anatomical evidence in the detection of the earliest wildfires. *Palaios* 19(2):113–128.
49. Glasspool IJ, Edwards D, Axe L (2006) Charcoal in the Early Devonian: A wildfire-derived Konservat–Lagerstätte. *Rev Palaeobot Palynol* 142(3–4):131–136.
50. Pflug HD, Prossl KF (1989) Palynology in gneiss—Results from the continental deep drilling program. *Naturwissenschaften* 76(12):565–567.
51. Pflug HD, Prössl KF (1991) Palynostratigraphical and paleobotanical studies in the pilot hole of the German continental deep drilling programme results and implications. *Sci Drill* 2(1):13–33.
52. Wollenweber J, et al. (2006) Characterisation of non-extractable macromolecular organic matter in Palaeozoic coals. *Palaeogeogr Palaeoclimatol Palaeoecol* 240(1–2): 275–304.
53. Peppers RA, Damberger HH (1969) *Palynology and Petrography of a Middle Devonian Coal in Illinois* (Illinois State Geological Survey, Urbana, IL).
54. Ammosov II (1964) Petrographic composition of coals in the U. S. S. R. and some of its changes. *Int Geol Rev* 6(10):1798–1804.
55. Volkova IB (1994) Nature and composition of the Devonian coals of Russia. *Energy Fuels* 8(6):1489–1493.
56. Patrakov YF, Kamyanov VF, Fedyaeva ON (2005) A structural model of the organic matter of Barzas liptobiolith coal. *Fuel* 84(2–3):189–199.
57. Sharypov VI, Kuznetsov BN, Beregovtsova NG, Startsev AN, Parmon VN (2006) Catalytic hydroliquefaction of Barzass liptobiolitic coal in a petroleum residue as a solvent. *Fuel* 85(7–8):918–922.
58. Ghori KAR (1999) *Silurian-Devonian Petroleum Source-Rock Potential and Thermal History, Carnarvon Basin, Western Australia* (Geological Survey of Western Australia, Perth, Australia).
59. Xu H-H, et al. (2012) Mid Devonian megaspores from Yunnan and North Xinjiang, China: Their palaeogeographical and palaeoenvironmental significances. *Palaeoworld* 21(1): 11–19.
60. Yang Y, Zou R, Shi Z, Jiang R (1996) *Atlas for Coal Petrography of China* (China Univ of Mining and Technology Press, Beijing).
61. Dai S, Han D, Chou C-L (2006) Petrography and geochemistry of the Middle Devonian coal from Luquan, Yunnan Province, China. *Fuel* 85(4):456–464.
62. Goodarzi F, Gentzis T, Embry AF (1989) Organic petrology of two coal-bearing sequences from the Middle to Upper Devonian of Melville Island, Arctic Canada. Working paper (Geological Survey of Canada, Ottawa). Available at ftp.maps.canada.ca/pub/nrcan_rncan/publications/ess_sst/126/126737/pa_89_08.pdf.
63. Goodarzi F, Goodbody Q (1990) Nature and depositional environment of Devonian coals from western Melville Island, Arctic Canada. *Int J Coal Geol* 14(3):175–196.
64. Gentzis T, Goodarzi F (1991) Petrology, depositional environment and utilization potential of Devonian channel coals from Melville Island, Canadian Arctic Islands. *Bull Soc Geol Fr* 162(2):239–253.
65. Fowler MG, Goodarzi F, Gentzis T, Brooks PW (1991) Hydrocarbon potential of Middle and Upper Devonian coals from Melville Island, Arctic Canada. *Org Geochem* 17(6): 681–694.
66. Michelsen JK, Khorasani GK (1991) A regional study on coals from Svalbard; Organic facies, maturity and thermal history. *Bull Soc Geol Fr* 162(2):385–397.
67. Rimmer SM, Thompson JA, Goodnight SA, Robl TL (2004) Multiple controls on the preservation of organic matter in Devonian–Mississippian marine black shales: Geochemical and petrographic evidence. *Palaeogeogr Palaeoclimatol Palaeoecol* 215(1–2):125–154.
68. Marynowski L, Filipiak P (2007) Water column euxinia and wildfire evidence during deposition of the Upper Famennian Hangenberg event horizon from the Holy Cross Mountains (central Poland). *Geol Mag* 144(03):569–595.
69. Cressler WL (2001) Evidence of earliest known wildfires. *Palaios* 16(2):171–174.
70. Rowe NP, Jones TP (2000) Devonian charcoal. *Palaeogeogr Palaeoclimatol Palaeoecol* 164(1–4):331–338.
71. Fairon-Demaret M, Hartkopf-Fröder C (2004) Late Famennian plant mesofossils from the Refrath 1 Borehole (Bergisch Gladbach-Paffrath Syncline; Ardennes-Rhenish Massif, Germany). *CFS Courier Forschungsinstitut Senckenberg* 251:89–121.
72. Prestianni C, Decombeix A-L, Thorez J, Fokan D, Gerrienne P (2010) Famennian charcoal of Belgium. *Palaeogeogr Palaeoclimatol Palaeoecol* 291(1–2):60–71.
73. Zhou L, et al. (2011) A new paleoenvironmental index for anoxic events—Mo isotopes in black shales from Upper Yangtze marine sediments. *Sci China Earth Sci* 54(7): 1024–1033.
74. Herrmann AD, et al. (2012) Anomalous molybdenum isotope trends in Upper Pennsylvanian euxinic facies: Significance for use of δ98Mo as a global marine redox proxy. *Chem Geol* 324–325:87–98.
75. Goldberg T, et al. (2013) Resolution of inter-laboratory discrepancies in Mo isotope data: An intercalibration. *J Anal At Spectrom* 28(5):724–735.
76. Nägler TF, et al. (2014) Proposal for an international molybdenum isotope measurement standard and data representation. *Geostand Geoanal Res* 38(2):149–151.
77. Canfield DE, Poulton SW, Narbonne GM (2007) Late-Neoproterozoic deep-ocean oxygenation and the rise of animal life. *Science* 315(5808):92–95.
78. Scott C, Lyons TW (2012) Contrasting molybdenum cycling and isotopic properties in euxinic versus non-euxinic sediments and sedimentary rocks: Refining the paleoproxies. *Chem Geol* 324–325:19–27.
79. Dahl TW, et al. (2013) Tracing euxinia by molybdenum concentrations in sediments using handheld X-ray fluorescence spectroscopy (HHXRF). *Chem Geol* 360–361: 241–251.
80. Chapin FS, Johnson DA, McKendrick JD (1980) Seasonal movement of nutrients in plants of differing growth form in an Alaskan tundra ecosystem: Implications for herbivory. *J Ecol* 68(1):189–209.
81. Chapin FS (1989) The cost of tundra plant structures: Evaluation of concepts and currencies. *Am Nat* 133(1):1–19.
82. Chapin FS, Shaver GR (1989) Differences in growth and nutrient use among Arctic plant growth forms. *Funct Ecol* 3(1):73–80.
83. Shaver GR, Chapin FS (1991) Production: Biomass relationships and element cycling in contrasting Arctic vegetation types. *Ecol Monogr* 61(1):1–31.
84. Aerts R, Verhoeven JTA, Whigham DF (1999) Plant-mediated controls on nutrient cycling in temperate fens and bogs. *Ecology* 80(7):2170–2181.
85. Riis T, Olesen B, Katborg CK, Christoffersen KS (2010) Growth rate of an aquatic bryophyte (Warnstorfia fluitans (Hedw.) Loeske) from a high Arctic lake: Effect of nutrient concentration. *Arctic* 63(1):100–106.
86. Waite M, Sack L (2011) Does global stoichiometric theory apply to bryophytes? Tests across an elevation × soil age ecosystem matrix on Mauna Loa, Hawaii. *J Ecol* 99(1): 122–134.
87. Wang M, Moore T (2014) Carbon, nitrogen, phosphorus, and potassium stoichiometry in an ombrotrophic peatland reflects plant functional type. *Ecosystems (N Y)* 17(4): 673–684.
88. Larmola T, et al. (2014) Methanotrophy induces nitrogen fixation during peatland development. *Proc Natl Acad Sci USA* 111(2):734–739.
89. Delgado V, Ederra A, Santamaría JM (2013) Nitrogen and carbon contents and δ(15) N and δ(13) C signatures in six bryophyte species: Assessment of long-term deposition changes (1980-2010) in Spanish beech forests. *Glob Change Biol* 19(7):2221–2228.
90. Elbert W, et al. (2012) Contribution of cryptogamic covers to the global cycles of carbon and nitrogen. *Nat Geosci* 5(7):459–462.
91. Royer DL, Donnadieu Y, Park J, Kowalczyk J, Goddéris Y (2014) Error analysis of CO2 and O2 estimates from the long-term geochemical model GEOCARBSULF. *Am J Sci* 314(9):1259–1283.